small
NANO MICRO

Functionalized MoS_2 Nanosheet-Based Field-Effect Biosensor for Label-Free Sensitive Detection of Cancer Marker Proteins in Solution

*Lu Wang, Ye Wang, Jen It Wong, Tomás Palacios, Jing Kong, and Hui Ying Yang**

Cancer is a leading cause of death worldwide, accounting for 7.6 million deaths (around 13% of all deaths) in 2008, and the number is projected to continue rising, with an estimated 13.1 million deaths in 2030.[1] A significant proportion of cancers can be cured, by surgery, radiotherapy or chemotherapy, especially if they are detected early. Biomarker is a biological molecule found in blood, other body fluids, or tissues, and its abnormal concentration is a sign of abnormal process or disease; biomedical research has elucidated many biomarkers that could greatly improve early disease diagnosis.[2] For example, prostate-specific antigen (PSA) was one of the first cancer biomarkers identified and put into routine clinical use for screening and diagnosis of prostate cancer,[3] the second most common cancer occurred in men worldwide.[1] The use of biosensors in the detection of cancer markers at the earliest stage is of paramount importance to cancer diagnostics and treatments.[4] A biosensor is an integrated device combining a biorecognition element with a transducer, which transforms the interactions between the biorecognition element and the specific target (for example, cancer marker proteins) to an output signal measured and displayed by a processor.[5] Compared to label-free detection methods, conventional label-based detection methods, for example, the enzyme-linked immunosorbent assay (ELISA), have drawbacks including complexity in sample processing, higher operational costs, lack of portability, and limited applications in real-time monitoring.[6,7]

In recent years, owing to the fast advances in nanotechnology, label-free biosensors based on nanoscale materials and structures with novel properties have been demonstrated, which outperformed the traditional methods in almost all aspects of a biosensor, such as detection speed, sensitivity, cost, and versatility.[8–14] However, synthesizing biosensors that simultaneously meet all these criteria has proven challenging. Although one-dimensional (1D) semiconductors, such as semiconductor nanowires,[8,10,12] and carbon nanotubes,[9,12,13] are usually the preferred channel materials for field-effect transistor (FET)-based biosensors, the emerging two-dimensional (2D) graphene sheets are also explored due to their large active surface area, which enhances the adsorption of target molecules, and their extreme thinness (only one atom thick),[11,15–18] which enables low-noise operation. However, graphene lacks bandgap, which adds a large leakage current and reduces dynamic range of the sensor. Other 2D nanomaterials such as transition metal dichalcogenides, for example, molybdenum disulfide (MoS_2),[19,20] have also attracted significant research interests. In contrast to graphene, MoS_2 has a direct energy bandgap which significantly lowers the leakage current.[21] When single-layer MoS_2 was employed as the active materials with HfO_2 as gate dielectric in FETs, a high current On/Off ratio exceeding 1×10^8 at room temperature has been demonstrated.[22] Fabrication of MoS_2 nanosheet-based field-effect transistors as NO gas sensor,[23,24] and chemical vapor sensor have been reported.[25] MoS_2 nanosheet-based FET are thus expected to be a potential candidate for biosensing, but no relevant studies have been demonstrated to the best of our knowledge.

In this paper, we report a label-free sensitive biosensor platform using multi-layer molybdenum disulfide (MoS_2) field-effect devices for cancer marker protein detection, which is the first demonstration on the biofunctionalization of MoS_2 nanosheet field-effect device and the application of the sensor in liquid-phase. The change in the MoS_2 transistor drain current was caused by the specific binding of cancer marker proteins, prostate-specific antigens (PSA), to the antibodies that were immobilized onto the MoS_2 film surface.[3] From our experimental results, our detection method features high sensitivity and almost instant detection feedback for PSA. In addition to the sub-picomolar sensitivity, the sensor appeared to have good specificity by showing no significant signals to non-target serum protein. This study demonstrates that biofunctionalized MoS_2 field-effect device is a promising candidate for the detection of cancer markers to advance the early cancer diagnostics.

L. Wang[+]
Department of Chemistry and Chemical Biology
Harvard University
Cambridge, MA, 02138, USA
Y. Wang,[+] J. I. Wong, H. Y. Yang
Pillar of Engineering Product Development
Singapore University of Technology and Design
138682, Singapore
E-mail: yanghuiying@sutd.edu.sg
Tel.: +65 6303 6663; Fax: +65 6779 5161
T. Palacios, J. Kong
Department of Electrical Engineering and Computer Science
Massachusetts Institute of Technology
Cambridge, Massachusetts 02139, USA
[+]These two authors contributed equally to this work

DOI: 10.1002/smll.201302081

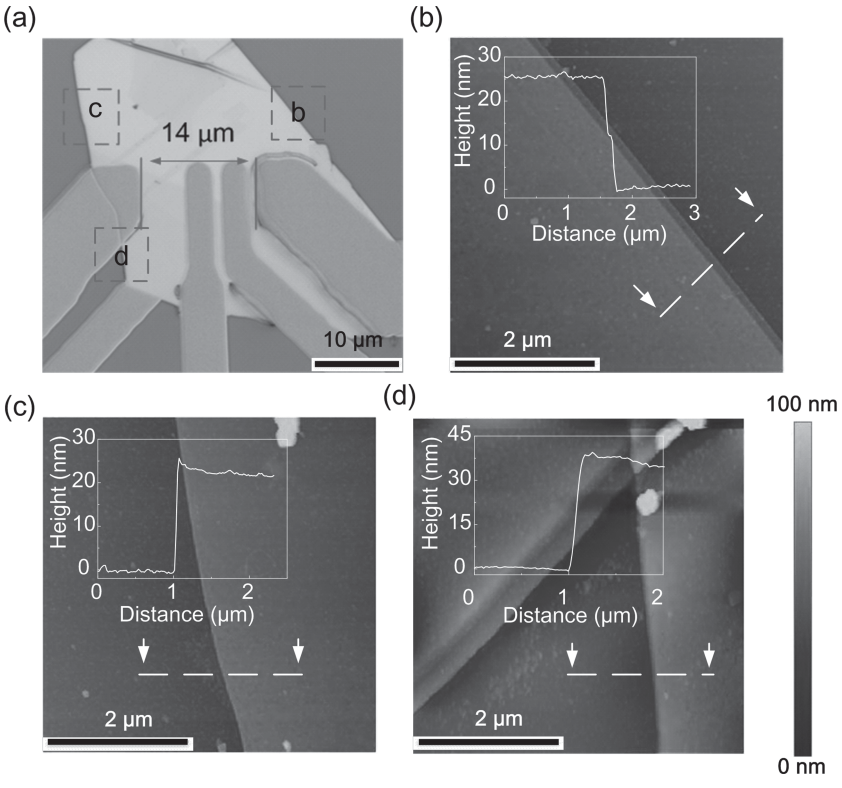

Figure 1. MoS_2 nanosheet-based field-effect device. (a) Optical image of the MoS_2 nanosheet-based field-effect device before HfO_2 deposition: the mechanically exfoliated multi-layer MoS_2 shows clear contrast compared to the substrate of 285 nm thick SiO_2 thermally grown on silicon; the source and drain electrodes are the two distant electrodes, marked out with arrows in the image. (b, c, d) AFM images and scanning traces of the device along the dotted lines in the regions indicated in Figure 1a: the height difference is the thickness of the multi-layer MoS_2.

The optical image of the MoS_2 device is shown in **Figure 1**a, with the multilayer MoS_2 structure showing distinguishable contrast on the Si/SiO_2 substrates. The two distant electrodes were chosen as the source and drain electrodes because the middle electrodes were damaged during fabrication, and this resulted in a device channel width of around 14 μm. The atomic force microscopy (AFM) image of the device was taken to determine the thicknesses of MoS_2 nanosheets; because the HfO_2 layer was homogenously covering the whole surface of the chip, the height difference measured at the edge of MoS_2 sheet indicates its thickness. Line profiles, measured at different parts around the MoS_2 sheet as marked in Figure 1a, were shown in Figure 1b-d, and the average thickness of the MoS_2 sheet used in this device is around 28 nm. It is noted that HfO_2 not only serves as the gate dielectric layer for the FET device, but also protects the metal electrodes from direct contact with liquid environment in biosensing and serves as the starting layer for silane-based covalent biofunctionalization.

Figure 2 shows the device transport characteristics in air. In the source-drain current (I_{ds}) versus backgate voltage (V_g) plot (Figure 2a), when the backgate voltage (V_g) increased and the source-drain voltage (V_{ds}) was kept constant at 0.1 V, the device current (I_{ds}) increased accordingly, which confirmed that we successfully obtained an n-type MoS_2 FET device. In addition, as shown in the I_{ds} vs V_{ds} plot (Figure 2b), when V_g was fixed at +0.1 V, the I_{ds}-V_{ds} plot was linear, indicating the contact between the MoS_2 and the metal electrodes was ohmic. The slight asymmetry in the negative and positive V_{ds} is probably due to the different numbers of layers of MoS_2 at the source and drain electrodes. To calculate the mobility μ, for the transistor in the linear region ($V_g - V_{th} \geq V_{ds}$, $V_g > V_{th}$), according to the equation

$$I_{ds} = \mu C_0 \frac{W}{L}\left[(V_g - V_{th})V_{ds} - \frac{V_{ds}^2}{2}\right] \quad (1)$$

where C_0 is the capacitance per unit area of the gate insulator and is 1.21×10^{-8} F for 285 nm thick SiO_2, V_g is the gate bias, V_{th} is the threshold voltage, V_{ds} is 0.1 V in our measurement, W and L are the width and length of the channel. According to the $I_{ds} - V_g$ plot and plugging W/L = 4/16, the mobility is calculated to be 6.6 $cm^2\ V^{-1}\ s^{-1}$. The mobility is lower than ~200 $cm^2\ V^{-1}\ s^{-1}$ obtained from the single layer MoS_2.[22] The possible reason may be due to the scattering from the trap states and impurities located at the interface between SiO_2 dielectric layer and MoS_2 channel layer.[26] The field effect mobility of MoS_2 field effect transistor has been reported to vary from 0.03 to 700 $cm^2\ V^{-1}\ s^{-1}$.[24,27,28] And our value is comparable with the previous results from the MoS_2 FET devices reported by other research groups.[24,26,29]

In addition to device transport characterization via backgate in air, we measured water-gate electrical characteristics, because it is closer to the liquid working condition of

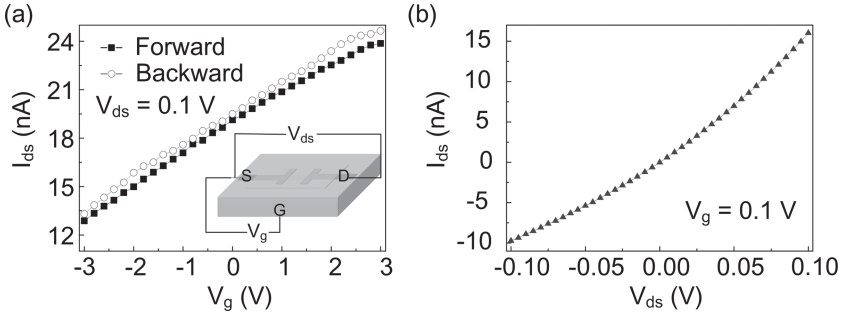

Figure 2. Transport properties of the n-type MoS_2 nanosheet-based field-effect device in air via backgate. (a) The dependance of source-drain current I_{ds} on the backgate V_g at a constant source-drain voltage V_{ds} of 0.1 V; inset: the schematic of the backgate measurement configuration. (b) The linear I_{ds} v.s. V_{ds} plot at a constant V_g of +0.1 V indicated the ohmic contact between the MoS_2 and the metal electrodes.

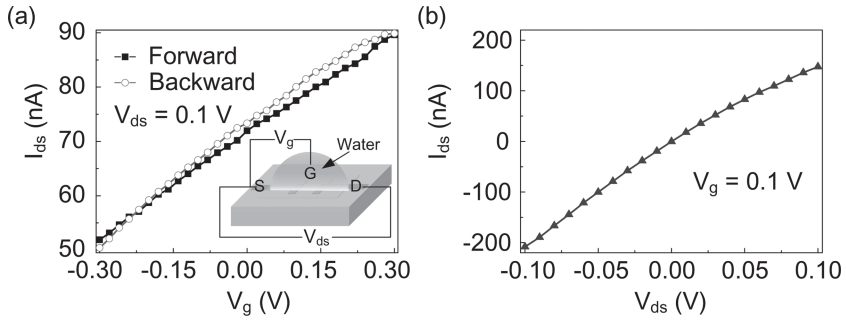

Figure 3. Watergate electrical characteristics of the n-type MoS_2 nanosheet-based field-effect device via Ag/AgCl wire in contact with the water. (a) The dependance of source-drain current I_{ds} on the watergate V_g at a constant source-drain voltage V_{ds} of 0.1 V; inset: the schematic of the watergate measurement configuration. (b) The linear I_{ds} v.s. V_{ds} plot at a constant V_g of +0.1 V confirmed that the ohmic contact between the MoS_2 and the metal electrodes stay intact under water.

biosensor. With Ag/AgCl wire as watergate electrode in contact with DI water which covered the device area, we swept the water-gate potential (V_g) and measured the change in source-drain current (I_{ds}), and the result is shown in **Figure 3**a. When V_g was changed from –0.3 V to +0.3 V and V_{ds} was kept at 0.1 V, I_{ds} changed from 52 nA to 90 nA, showing n-type device characteristics. It is worth mentioning that a field-effect device can perform bio-sensing in linear regime, near threshold regime or subthreshold/depletion regime.[30] In our experiment, the device worked in the linear regime (the drain current varied with gate voltage linearly) for biosensing. Moreover, as shown in the I_{ds}-V_{ds} plot (Figure 3b), when V_g was fixed at +0.1 V, the I_{ds}-V_{ds} curve was linear, indicating that the device kept its ohmic contacts in liquid environment.

Upon successful fabrication of MoS_2 field-effect devices with decent transport characteristics, in order to transform the device into a biological sensor, the device was biofunctionalized with recognition elements that specifically bind with target biological analytes. In our experiments, we chose prostate-specific antigen (PSA),[3] one of the first cancer biomarkers identified and put into routine clinical use for screening and diagnosis of prostate cancer, as the target analytes, and the monoclonal anti-PSA antibody as the recognition element. When the antibodies attached on the device surface specifically bind with PSA molecules in the solution, the binding events give rise to detectable electrical signals in terms of source-drain current changes according to field-effect mechanism.

The biofunctionalization strategy was to modify the HfO_2 layer covering the MoS_2 surface with silane molecules to present surface aldehyde groups, which further react with amino groups in the anti-PSA antibodies, following the procedures modified from the literature.[31–38] Silane-based covalent coupling of monoclonal antibodies was chosen because it has the following advantages: (1) surface hydroxyl groups of HfO_2 are readily available for coupling to silane coupling agents;[39] (2) there are a variety of functional groups available at the other end of the coupling agents to react and connect with different recognition elements, making this strategy a versatile way for various sensing targets; (3) the coupling reagents are covalently attached to both the device surface and the antibodies, and this stable and irreversible modification is especially helpful in flowing sensing system to minimize the loss of binding sites and for a longer sensor life-time.

The MoS_2 field-effect based sensing of prostate cancer marker protein PSA was performed in a homebuilt microfluidic channel system, as shown in **Figure 4**a and 4b, where different sample solutions can be flowed into the channel consecutively to interact with the active area of the device. A syringe pump (PHD2000, Harvard Apparatus) was used to draw the solution from different vials into the microfluidic channel at a speed of 0.3 mL per hour. Because of the screening effect on charges in electrolyte solutions,[40] the sensing experiment was carried out in 100 μM phosphate buffer solutions with Debye length ~25 nm and the pH was 6.68. The source-drain voltage V_{ds} of –0.1 V and water-gate voltage V_g of 0.3 V were used. When positively charged PSA (pI 6.8 in pH 6.68 sensing buffer) binds to antibody receptors on the surface of MoS_2 device, it acts as a positive gate potential applied on the device surface, and the conductance of n-type field-effect device increases accordingly.

The transport characteristics of the device after biofunctionalization was measured in buffer solution via Ag/AgCl wire electrode, and the I_{ds}-V_g plot is shown in **Figure 5**a. When V_g was changed from –0.1 V to +0.4 V and V_{ds} was kept at –0.1 V, I_{ds} changed from ~0 nA to –8 nA, showing n-type device characteristics. We chose to use V_g = +0.3 V throughout the biosensing measurement because the device was in the linear regime around this gate voltage. It is worth mentioning that before the bio-functionalization, the device was in the linear regime when watergate was in the

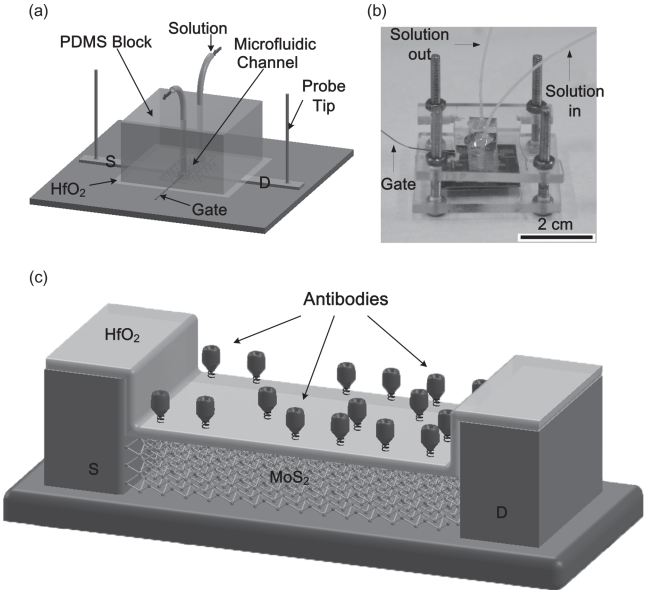

Figure 4. Schematic (a) and photo (b) of the biosensor configuration. (c) Schematic of the biofunctionalization layers on the device surface (S: source, D: drain).

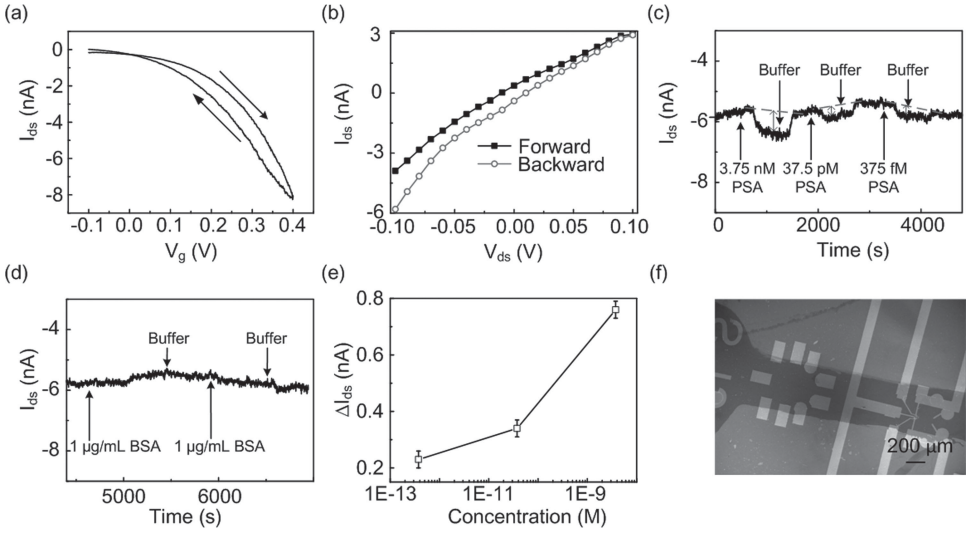

Figure 5. Real-time detection of prostate specific antigen (PSA) with MoS_2 nanosheet-based field-effect biosensor. (a) Device transport characteristics (source-drain current I_{ds} v.s. water-gate voltage V_g) in solution after the biofunctionalization, with souce-drain voltage V_{ds} fixed at –0.1 V. (b) I_{ds}-V_{ds} with water-gate voltage V_g at +0.3 V. (c) Conductance-versus-time data recorded during alternate delivery of PSA and pure buffer solutions; the PSA concentrations were 3.75 nM, 37.5 pM and 375 fM, respectively. Dashed lines are the local baselines, and the length of the lines with arrows are the ΔI_{ds} (i.e., I_{ds} change in response to the presence of PSA). The buffer solutions used in all measurements were 100 μM phosphate buffer solutions. (d) Control sensing experiment with high concentration BSA (1 ug/mL, i.e., 15 nM). (e) The dependence of ΔI_{ds} on the concentration of PSA. (f) SEM image of the sensor chip after biosensing test.

–0.3 V~+0.3 V range as shown in Figure 3a. However, after the bio-functionalization, the charged biomaterial layer shifted the I_{ds}-V_g curve (Figure 5a), and the n-type device was turned off around 0 V. The significant change in the I_{ds}-V_g curve served as strong evidence for the succesfully immoblized biomaterial layer. Moreover, as shown in the I_{ds}-V_{ds} plot (Figure 5b), when V_g was fixed at +0.3 V, the I_{ds}-V_{ds} curve was linear, indicating that the device kept its ohmic contacts intact after biofunctionalization in liquid solutions.

As shown in Figure 5c, the device conductance increased (i.e. an increase in the absolute value of I_{ds} at the constant V_{ds} of –0.1 V), as expected,when PSA solutions with various concentrations (3.75 nM, 37.5 pM and 375 fM, respectively) were delivered into the microfluidic channel and PSA molecules binded with the antibodies immobilized on the device surface. And then the device showed the reversible conductance changes (i.e. I_{ds} came back to the baseline current) when the buffer was introduced for the reversible unbinding of PSA molecules off the device surface. Note that the arrows in Figure 5c and 5d mark the time points when the rear end of the tubing switches to a new solution (PSA or buffer solutions), and because it takes time (around 200–250 s) for the new solution to travel from the rear end of the tubing to the inlet of the microchannel in the PDMS block, the conductance changes appear when the solution flows into the microchannel which is at a later time than that marked by the arrows. Furthermore, the change in device drain current (ΔI_{ds}) is dependent on the concentration of the PSA solution, and the concentration-dependence is summarized in Figure 5e. The ΔI_{ds} was determined by using the local current baseline (dashed lines in Figure 5c) and measuring the distance between the baseline and the bottom of the I_{ds} curve in response to PSA (the distances are shown as lines with arrows in Figure 5c). The ΔI_{ds} for PSA concentrations of 3.75 nM, 37.5 pM and 375 fM are 0.76 nA, 0.34 nA, and 0.23 nA, respectively. The biosensor demonstrated good sensitivity by showing clear signals to PSA solution with the concentration down to 375 fM, as well as high selectivity by showing no response to 1 ug/mL (i.e., 15 nM) Bovine Serum Albumin (BSA) solution as shown in Figure 5d.

In conclusion, we achieved label-free real-time detection of cancer marker protein PSA with high sensitivity and selectivity, using multi-layer MoS_2 nanosheet-based field-effect device with versatile HfO_2-silane-based bio-functionalization scheme, which promises their wide application in detection of other disease markers and the potential for point-of-care diagnostics.

Experimental Section

Device Fabrication: The FET fabrication process started with the mechanical exfoliation of multilayer MoS_2 films from bulk MoS_2 (SPI Supplies),[22,41,42] which were then transferred to 285 nm thick SiO_2 thermally grown on silicon substrates, referred to as Si/SiO_2. Conventional photolithography followed by thermal evaporation of metal electrical contacts were used to fabricate multilayer MoS_2 FET devices. The metal contacts are 5/70 nm thick Ti/Au, with Ti layer for good adhesion between gold and substrate. The devices were subsequently thermally annealed at 200 °C under Ar/H_2 (100/10 sccm) gas flow for one hour to facilitate the formation of Ohmic contacts and remove residual organic contaminants during the fabrication process. Then, a 7–8 nm thick hafnium oxide (HfO_2) as the high-*k* gate dielectric was deposited to cover the device chip at 250 °C by atomic layer deposition (ALD).[22,43]

Biofunctionalization: The biofunctionalization process was modified based on the method reported by Kim et al. and other

NANO MICRO small

research groups.[31–38] In brief, the prepared chip was cleaned by oxygen plasma at 40 W for 1 min. After that, the chip was immersed into the 3-Triethoxysilylpropylamine (APTES) solution (0.1 ml APTES dropped into 10 ml 95%/5% ethanol/water solution) for 45 mins. Then the chip was gently washed by isopropanol (IPA), blown dry by N_2 gas, and baked on a hotplate at 115 °C for 5 mins. After APTES modification, the chip was put into glutaraldehyde solution (2.5%, Sigma G6403) in coupling buffer (CB) containing $NaCNBH_4$ (6 mM, Sigma 156159) for 2 hours, followed by rinsing with deionized (DI) water, acetone and IPA. The CB solution was prepared by putting one phosphate buffered saline tablet (Sigma P4417) into DI water (200 ml), and the pH was adjusted to 7.9 by adding NaOH solution. Then the chip was immersed into antibody (100 ug) binding buffer (BB) (1 mL) containing $NaCNBH_4$ (6 mM). The BB solution was prepared by adding $Na_2HPO_4{\cdot}7H_2O$ (260 mg, Sigma S9390) and $NaH_2PO_4{\cdot}1H_2O$ (4 mg, Sigma S9638) in DI water (100 mL).

Device Assembly: A PDMS block with a microfluidic channel (500 μm in width, 70 μm in height and 13 mm in length) was employed to cover the MoS_2 device area on top of the HfO_2 layer. Two PTFE tubes with diameter of 0.3 mm were used as the inlet and outlet for delivering solutions. A Ag/AgCl wire was inserted into the PDMS block to be in contact with the liquid in the microfluidic channel.

Characterization: The surface morphology was performed by a Nano Scope IIIa Atomic Force Microscopy (AFM). Electrical characterizations of the fabricated MoS_2 FETs were conducted both in air via SiO_2/Si backgate and in liquid solution via Ag/AgCl wire in contact with the solution, using a Keithley 4200 semiconductor characterization system with a probe station at room temperature.

Acknowledgements

This work is supported by Singapore University of Technology and Design, International Design Center (IDC) grant to Dr. Yang Hui Ying (Grant No. IDG11000101).

[1] J. Ferlay, H. R. Shin, F. Bray, D. Forman, C. Mathers, D. M. Parkin, GLOBOCAN 2008, Cancer Incidence and Mortality Worldwide: IARC CancerBase No. 10 International Agency for Research on Cancer, Lyon, France, **2010**, *29*.
[2] R. Etzioni, N. Urban, S. Ramsey, M. McIntosh, S. Schwartz, B. Reid, J. Radich, G. Anderson, L. Hartwell, *Nat. Rev. Cancer* **2003**, *3*, 243–252.
[3] D. S. Smith, P. A. Humphrey, W. J. Catalona, *Cancer* **1997**, *80*, 1852–1856.
[4] B. Bohunicky, S. A. Mousa, *Nanotechnol. Sci. Appl.* **2011**, *4*, 1–10.
[5] D. R. Thévenot, K. Toth, R. A. Durst, G. S. Wilson, *Biosens. Bioelectron.* **2001**, *16*, 121–131.
[6] A. M. Ward, J. Catto, F. Hamdy, *Ann. Clin. Biochem.* **2001**, *38*, 633–651.
[7] B. E. Rapp, F. J. Gruhl, K. Länge, *Anal. Bioanal. Chem.* **2010**, *398*, 2403–2412.
[8] F. Patolsky, G. Zheng, C. M. Lieber, *Nanomedicine* **2006**, *1*, 51–65.
[9] X. Tang, S. Bansaruntip, N. Nakayama, E. Yenilmez, Y.-l. Chang, Q. Wang, *Nano Lett.* **2006**, *6*, 1632–1636.
[10] E. Stern, J. F. Klemic, D. A. Routenberg, P. N. Wyrembak, D. B. Turner-Evans, A. D. Hamilton, D. A. LaVan, T. M. Fahmy, M. A. Reed, *Nature* **2007**, *445*, 519–522.
[11] N. Mohanty, V. Berry, *Nano Lett.* **2008**, *8*, 4469–4476.
[12] C. Li, M. Curreli, H. Lin, B. Lei, F. Ishikawa, R. Datar, R. J. Cote, M. E. Thompson, C. Zhou, *J. Am. Chem. Soc.* **2005**, *127*, 12484–12485.
[13] P. Hu, J. Zhang, L. Li, Z. Wang, W. O'Neill, P. Estrela, *Sensors* **2010**, *10*, 5133–5159.
[14] W. Yang, K. R. Ratinac, S. P. Ringer, P. Thordarson, J. J. Gooding, F. Braet, *Angew. Chem. Int. Ed.* **2010**, *49*, 2114–2138.
[15] K. S. Novoselov, A. K. Geim, S. Morozov, D. Jiang, Y. Zhang, S. Dubonos, I. Grigorieva, A. Firsov, *Science* **2004**, *306*, 666–669.
[16] A. K. Geim, K. S. Novoselov, *Nat. Mater.* **2007**, *6*, 183–191.
[17] Y. Zhu, S. Murali, W. Cai, X. Li, J. W. Suk, J. R. Potts, R. S. Ruoff, *Adv. Mater.* **2010**, *22*, 3906–3924.
[18] Y. Liu, X. Dong, P. Chen, *Chem. Soc. Rev.* **2012**, *41*, 2283–2307.
[19] R. F. Frindt, *J. Appl. Phys.* **1966**, *37*, 1928.
[20] H. Li, Q. Zhang, C. C. R. Yap, B. K. Tay, T. H. T. Edwin, A. Olivier, D. Baillargeat, *Adv. Funct. Mater.* **2012**, *22*, 1385–1390.
[21] K. F. Mak, C. Lee, J. Hone, J. Shan, T. F. Heinz, *Phys. Rev. Lett.* **2010**, *105*, 136805.
[22] B. Radisavljevic, A. Radenovic, J. Brivio, V. Giacometti, A. Kis, *Nat. Nanotechnol.* **2011**, *6*, 147–150.
[23] Q. He, Z. Zeng, Z. Yin, H. Li, S. Wu, X. Huang, H. Zhang, *Small* **2012**, *8*, 2994–2999.
[24] H. Li, Z. Y. Yin, Q. Y. He, X. Huang, G. Lu, D. W. H. Fam, A. I. Y. Tok, Q. Zhang, H. Zhang, *Small* **2012**, *8*, 63–67.
[25] F. Perkins, A. Friedman, E. Cobas, P. Campbell, G. Jernigan, B. Jonker, *Nano Lett.* **2013**, *13*, 668–673.
[26] Z. Y. Yin, H. Li, L. Jiang, Y. M. Shi, Y. H. Sun, G. Lu, Q. Zhang, X. D. Chen, H. Zhang, *ACS Nano* **2012**, *6*, 74–80.
[27] D. J. Late, B. Liu, H. R. Matte, V. P. Dravid, C. Rao, *ACS Nano* **2012**, *6*, 5635–5641.
[28] S. Das, H.-Y. Chen, A. V. Penumatcha, J. Appenzeller, *Nano Lett.* **2012**, *13*, 100–105.
[29] H. Wang, L. Yu, Y.-H. Lee, Y. Shi, A. Hsu, M. L. Chin, L.-J. Li, M. Dubey, J. Kong, T. Palacios, *Nano Lett.* **2012**, *12*, 4674–4680.
[30] X. P. Gao, G. Zheng, C. M. Lieber, *Nano Lett.* **2009**, *10*, 547–552.
[31] A. Kim, C. S. Ah, H. Y. Yu, J.-H. Yang, I.-B. Baek, C.-G. Ahn, C. W. Park, M. S. Jun, S. Lee, *Appl. Phys. Lett.* **2007**, *91*, 103901.
[32] J. H. Chua, R.-E. Chee, A. Agarwal, S. M. Wong, G.-J. Zhang, *Anal. Chem.* **2009**, *81*, 6266–6271.
[33] M.-H. Lee, K.-N. Lee, S.-W. Jung, W.-H. Kim, K.-S. Shin, W.-K. Seong, *Int. J. Nanomed.* **2008**, *3*, 117–142.
[34] M. Lin, C. Chu, L. Tsai, H. Lin, C.-S. Wu, Y. Wu, Y. Wu, D.-B. Shieh, Y. Su, C. Chen, *Nano Lett.* **2007**, *7*, 3656–3661.
[35] G.-J. Zhang, L. Zhang, M. J. Huang, Z. H. H. Luo, G. K. I. Tay, E.-J. A. Lim, T. G. Kang, Y. Chen, *Sens. Actuators, B.* **2010**, *146*, 138–144.
[36] G. F. Zheng, F. Patolsky, Y. Cui, W. U. Wang, C. M. Lieber, *Nat. Biotechnol.* **2005**, *23*, 1294–1301.
[37] F. Patolsky, G. Zheng, C. M. Lieber, *Nat. Protoc.* **2006**, *1*, 1711–1724.
[38] G. MacBeath, S. L. Schreiber, *Science* **2000**, *289*, 1760–1763.
[39] E. P. Plueddemann, Silane coupling agents, Plenum Press, New York and London **1991**.
[40] E. Stern, R. Wagner, F. J. Sigworth, R. Breaker, T. M. Fahmy, M. A. Reed, *Nano Lett.* **2007**, *7*, 3405–3409.
[41] K. S. Novoselov, D. Jiang, F. Schedin, T. J. Booth, V. V. Khotkevich, S. V. Morozov, A. K. Geim, *Proc. Natl. Acad. Sci. USA* **2005**, *102*, 10451–10453.
[42] C. Lee, H. Yan, L. E. Brus, T. F. Heinz, J. Hone, S. Ryu, *ACS Nano* **2010**, *4*, 2695–2700.
[43] F. Chen, J. Xia, D. K. Ferry, N. Tao, *Nano Lett.* **2009**, *9*, 2571–2574.

Received: July 8, 2013
Revised: September 21, 2013
Published online: January 29, 2014

